COMPDYN 2009
ECCOMAS Thematic Conference on
Computational Methods in Structural Dynamics and Earthquake Engineering
M. Papadrakakis, N.D. Lagaros, M. Fragiadakis (eds.)
Rhodes, Greece, 22-24 June 2009

A HIGH-ORDER DOUBLY ASYMPTOTIC OPEN BOUNDARY CONDITION FOR SCALAR WAVES IN A WAVEGUIDE

S. Prempramote[1] and C. Song[2]

[1]University of New South Wales
School of Civil and Environmental Engineering, Sydney, NSW 2052, Australia
e-mail: suriyon@student.unsw.edu.au

[2] University of New South Wales
School of Civil and Environmental Engineering, Sydney, NSW 2052, Australia
e-mail: c.song@unsw.edu.au

Keywords: Open Boundary, Doubly Asymptotic, Continued Fraction, Wave Propagation, Absorbing Boundary, Transmitting Boundary.

Abstract. *A high-order doubly asymptotic open boundary condition is developed for the transient analyses of scalar waves propagating in a waveguide. An equation of the dynamic stiffness in the frequency domain of the waveguide is derived from its definition and the wave equation. A doubly asymptotic continued fraction solution of the dynamic stiffness is determined recursively. By introducing auxiliary variables, the open boundary condition is expressed as a system of first-order ordinary differential equations in time. The two time-independent coefficient matrices, the static stiffness and damping matrices, are symmetric and tri-diagonal. Well-established time-stepping schemes in structural dynamics are directly applicable. No other parameters than the orders of the low- and high-frequency expansions need to be selected by the users in the analysis. It is demonstrated analytically or numerically that*

1. *Several well-established high-order absorbing boundary conditions, such as Higdon's multi-directional boundary, are equivalent to the singly-asymptotic continued fraction solution at the high-frequency limit. The singly-asymptotic open boundary condition is unable to model evanescent waves below the cut-off frequency. In a long-time analysis, the singly-asymptotic open boundary condition suffers from numerical pollution similar to the "fictitious reflections" caused by simple boundary conditions.*

2. *The dynamic stiffness of the doubly-asymptotic open boundary condition converges rapidly to the exact solution in the frequency domain as its order increases. Evanescent waves and late-time (low-frequency) responses are also simulated accurately. Compared to the singly-asymptotic open boundary of the same order, the doubly-asymptotic open boundary shows a significant improvement in accuracy, i.e. no "fictitious reflections" occur.*

3. *The amount of computer time and storage required by the doubly-asymptotic open boundary condition are the same as those required by the singly-asymptotic open boundary condition of the same order.*

1 INTRODUCTION

When wave propagation problems are modeled, it is often necessary to introduce an artificial boundary around the region of interest so that the size of computational domain is limited to allow the application of well-established numerical methods such as the finite element method. The region exterior to the artificial boundary is regarded as an unbounded domain. A boundary condition mimicking the unbounded domain has to be enforced on the artificial boundary to prevent fictitious reflections that pollute the solution. A direct time-domain formulation of the boundary condition is required when nonlinearities occur in the region of interest. Such a boundary condition is known by various names such as absorbing, non-reflecting, open, radiation, transmitting and transparent boundary conditions. In this paper, only the term "open boundary" is employed to refer to the artificial boundary with a boundary condition mimicking the unbounded domain. Extensive literature on various open boundaries exists. Excellent literature reviews are available in papers [1, 2, 3, 4, 5, 6] and books [7, 8, 9, 10].

In theory, an exact open boundary is global in space and time, i.e. the present response at a point on the boundary is a function of the response history at all boundary points up to the present time. When a rigorous method (for example, the boundary element method [11, 12], the thin-layer method [13] or the scaled boundary finite-element method [10, 14]) is employed to construct an open boundary, the formulation is global. The convolution integral and storage of the response history are computationally expensive for large-scale problems and long-time calculations.

Time realization techniques have been proposed to construct temporally local open boundaries from the dynamic stiffness matrices obtained at discrete frequencies from analytical solution or by a rigorous method. In References [15, 16, 17], a Padé approximation of the dynamic stiffness matrix is constructed by using a curve fitting technique based on the least-squares method. A temporally local open boundary is formulated after expressing the Padé approximation as unit fractions. In Reference [18], the Padé approximation is expressed as a continued fraction leading to a mixed-variable method. In Reference [19], system theory is applied to construct a temporally local open boundary from the unit-impulse response obtained from the scaled boundary finite-element method.

Moreover, a large number of approximate open boundary conditions have been developed. Well-known examples include the viscous boundary [20], the superposition boundary [21], the paraxial boundary [22] and the extrapolation boundary [23]. Generally speaking, they are spatially and temporally local, i.e. the response at a point is coupled with the response at a few adjacent points during a few previous time steps only. These local open boundaries are simple and computationally efficient by themselves, but have to be applied to an artificial boundary sufficiently away from the region of interest in order to obtain results of acceptable accuracy. This increases the total computational effort.

To increase the accuracy and efficiency of simple open boundaries, high-order local open boundaries have been proposed. This type of open boundary has the potential of leading to accurate results as the order of approximation increases. At the same time, it is computationally efficient owing to its local formulation. Examples of early developments include the paraxial boundary [22], the Bayliss, Gunzburger and Turkel (BGT) boundary [24] and the multi-direction boundary [25]. However, the order of derivative in these formulations increases with the order of the open boundary. Beyond the second order, the implementation in a finite-element computer program becomes complex and instability may occur [8].

Researchers in several fields have shown their strong interest in developing open boundaries

of arbitrarily high order (see, e.g. [26, 27, 28, 29, 30, 31, 32]). Literature reviews are available, e.g., in References [4, 6]. Most of the open boundaries are, however, limited to straight, circular and spherical boundaries. Special corner conditions have to be devised for rectangular boundaries. Krenk [30] showed that several of well-established open boundaries can be formulated as a rational function approximation (Padé or continued fraction expansion) of the plane wave representation for scalar waves.

All the above high-order open boundaries were constructed to absorb propagating waves radiating energy. As they are singly asymptotic at the high-frequency limit, these high-order open boundaries are appropriate for radiative fields, i.e., virtually all of the field energy is propagating out to infinity [33]. In some classes of applications, a part of the total energy may be trapped near the region of interest and may not propagate to infinity. The best-known example is probably the evanescent waves occurring in a semi-infinite layer with a constant depth (also known as a waveguide). It is explained in Reference [34] that inclusion of evanescent modes improves the accuracy of the long-time behavior of a high-order open boundary. Another example is the class of problems where the dimensionless frequency $a_0 = \omega r_0/c$ (ω is the smallest excitation frequency of interest, r_0 is a characteristic length of the region of interest, c is the wave velocity) is very low (statics can be regarded as the limiting case $a_0 \to 0$). These wave fields are largely non-radiative. To achieve reasonably accurate results at low frequencies, i.e., over long time, the order of an open boundary has to be very high, thereby leading to large computational cost. In most of the publications on high-order open boundaries, the numerical results are shown for only the first few periods, and long-time responses are rarely reported.

From an application point of view, it is highly desirable to develop a temporally local open boundary that is capable of accurately mimicking an unbounded domain over the entire frequency range (i.e. from zero to infinity). One advance toward this objective is the introduction of the doubly-asymptotic boundaries [33, 35, 36, 37, 38]. This formulation is spatially global as the dynamic stiffness is exact not only at the high-frequency limit but also at statics. To the knowledge of the authors, the highest order reported is three [39].

Recently, a new approach to constructing temporally local open boundaries of arbitrarily high order has been proposed in Reference [40]. It is applicable to both scalar and vector waves. The geometry of the boundary of the unbounded domain can be arbitrary as long as the scaling requirement (there exists a zone from where the whole boundary is visible) is satisfied. Anisotropic unbounded media are handled without additional computation cost. Different from most of existing approaches, it seeks a continued fraction solution for the equation of the dynamic stiffness matrix of an unbounded domain obtained in the scaled boundary finite-element method [14]. Each term of the continued fraction is a linear function of the excitation frequency ω. The constant matrices in the continued fraction are determined recursively by satisfying the scaled boundary finite-element equation at the high-frequency limit. No explicit solution of the dynamic stiffness matrix at discrete frequencies is required. By using the continued fraction solution, the force-displacement relationship of the unbounded domain is formulated as a temporally local open boundary condition in the time domain. However, like other high-order open boundaries, this open boundary is inappropriate to model evanescent waves, and the convergence rate at low frequencies is much slower than that at high frequencies.

In this paper, a technique for constructing a high-order doubly asymptotic open boundary is proposed by extending the work in Reference [40]. Only scalar waves and an unbounded domain with simple geometry, namely a semi-infinite layer with a constant depth (a waveguide), are considered. The open boundary of a semi-infinite layer with a constant depth can be applied directly to solve practical problems by introducing a straight artificial boundary [17, 34]. The

investigations into the simple cases also provide insights into the basic numerical phenomena involved in high-order open boundaries such as the failure in representing evanescent waves and the relative poor performance at low frequencies. Furthermore, a novel approach to developing an efficient open boundary for the semi-infinite layer is proposed.

2 DYNAMIC STIFFNESS OF SEMI-INFINITE LAYER WITH CONSTANT DEPTH

The linear homogeneous scalar wave equation is expressed as

$$\nabla^2 u = \frac{1}{c^2}\ddot{u} \tag{1}$$

where $u = u(x, y, z, t)$ denotes the wave field, ∇^2 the Laplace operator and c the given wave speed. The initial conditions of an unbounded domain which is at rest are expressed as

$$u = \dot{u} = 0 \qquad \text{at } t = 0 \tag{2}$$

By employing the method of separation of variables, Eq. (1) can be transformed to a series of one-dimensional wave equations. From a one-dimensional wave equation and the definition of a dynamic stiffness coefficient, an equation of the dynamic stiffness coefficient is then derived.

A constant-depth h semi-infinite layer with the x-axis of the coordinate system that is aligned at the lower boundary of the layer is shown in Fig. 1. The formulation of the proposed open boundary is based on the dynamic stiffness representing the property of the semi-infinite layer and is independent of the coordinate system. The open boundary is thus applicable to semi-infinite layers of any orientation. A distributed traction $\tau_0(t)$ is assumed to be applied to the vertical boundary Γ_V (at $x = x_0$). The homogeneous boundary conditions prescribed on the parallel upper boundary Γ_U and lower boundary Γ_L are satisfied in the method of separation of variables by eigenfunctions. For example, when the upper boundary Γ_U is free (i.e. $u_{,y}(y = h) = 0$) and the lower boundary Γ_L is fixed (i.e. $u(y = 0) = 0$) the eigenfunctions are $\sin(\lambda_i y/h)$ where the eigenvalues are equal to $\lambda_i = (2i+1)\pi/2$ for $i = 0, 1, \ldots$. Note that as the eigenvalue λ_i increases, the eigenfunction varies more rapidly along the vertical boundary.

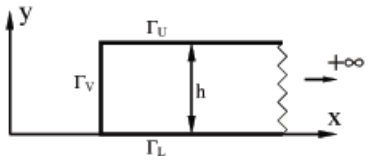

Figure 1: Semi-infinite layer with constant depth

For a mode with a modal eigenvalue λ, the one-dimensional wave equation is expressed as

$$\frac{\partial^2 \tilde{u}}{\partial x^2} - \left(\frac{\lambda}{h}\right)^2 \tilde{u} = \frac{1}{c^2}\ddot{\tilde{u}} \tag{3}$$

where $\tilde{u} = \tilde{u}(x,t)$ is the modal displacement. The modal traction is denoted as $\tilde{\tau}_0(t)$ at $x = x_0$. Once the solution of Eq. (3) satisfying both the boundary condition at $x = x_0$ and the radiation condition at $x \to +\infty$ is known, the solution for the wave propagation in the semi-infinite layer can be obtained by modal superposition. Hereafter, only the modal equation in Eq. (3) is addressed, and the word "modal" is omitted for the sake of simplicity except where confusion may arise.

By assuming the time-harmonic behavior $\tilde{u} = \widetilde{U}(\omega,x)\mathrm{e}^{+\mathrm{i}\omega t}$ and $\tilde{\tau}_0(t) = \widetilde{R}(\omega,x)e^{+\mathrm{i}\omega t}$ (ω is the excitation frequency), Eq. (3) is rewritten in the frequency domain as

$$\frac{\mathrm{d}^2\widetilde{U}}{\mathrm{d}x^2} + \frac{1}{h^2}\left(a_0^2 - \lambda^2\right)\widetilde{U} = 0 \tag{4}$$

where $\widetilde{U} = \widetilde{U}(\omega,x)$ is the displacement amplitude, and a_0 is a dimensionless frequency

$$a_0 = \frac{\omega h}{c} \tag{5}$$

2.1 Analytical solution

The solution of Eq. (4) satisfying the radiation condition for the semi-infinite layer extending to $x \to +\infty$ (Fig. 1) is

$$\widetilde{U} = C\mathrm{e}^{-\sqrt{\lambda^2 - a_0^2}x/h} \tag{6}$$

with the integration constant C. A cut-off frequency exists in Eq. (6) at the dimensionless frequency $a_0 = \lambda$. Below the cut-off frequency, i.e. $a_0 < \lambda$, the displacement decays exponentially. No propagating waves exist, in other words, evanescent waves are present. Above the cut-off frequency, i.e. $a_0 > \lambda$, Eq. (6) describes a wave propagating with a frequency-dependent phase velocity.

For the semi-infinite layer extending to the right-hand side, the force amplitude $\widetilde{R} = \widetilde{R}(\omega,x)$ on a vertical boundary at arbitrary x is expressed as

$$\widetilde{R} = -h\frac{\mathrm{d}\widetilde{U}}{\mathrm{d}x} \tag{7}$$

Substituting Eq. (6) into Eq. (7) results in

$$\widetilde{R} = -h\frac{\mathrm{d}\widetilde{U}}{\mathrm{d}x} = C\sqrt{\lambda^2 - a_0^2}\mathrm{e}^{-\sqrt{\lambda^2 - a_0^2}x/h} \tag{8}$$

The open boundary condition is represented as a force-displacement relationship. In the frequency domain, this relationship is defined by the dynamic stiffness coefficient $S = S(\omega,x)$ at a vertical line with a constant $x-$coordinate

$$\widetilde{R} = S\widetilde{U} \tag{9}$$

It is analogous to the DtN operator [41]. The solution for the dynamic stiffness coefficient can be obtained from its definition in Eq. (9) with the substitution of Eqs. (6) and (8)

$$S(a_0) = \sqrt{\lambda^2 - a_0^2} \tag{10}$$

Note that the dynamic stiffness coefficient $S(a_0)$ is only a function of the dimensionless frequency a_0 and is independent of the value of the x coordinate (Eq. (5)). Below the cut-off frequency, i.e. $a_0 < \lambda$, $S(a_0)$ is a real number whereas the imaginary part representing radiation damping vanishes. At the cut-off frequency $a_0 = \lambda$, $S(a_0)$ is equal to zero representing the resonance of the semi-infinite layer. Above the cut-off frequency, i.e. $a_0 > \lambda$, $S(a_0)$ is pure

imaginary. Equation (10) normalized by the modal eigenvalue λ is the square-root operator widely used in constructing open boundaries

$$\frac{S(a_0)}{\lambda} = \sqrt{1-\left(\frac{a_0}{\lambda}\right)^2} \tag{11}$$

To obtain a reference solution to validate numerical results in the time domain, the response to a unit impulse of traction $\tilde{\tau}_{0I}(t) = \delta(t)$ ($\delta(t)$ represents the Dirac-delta function) applied at $x = x_0$ is evaluated. The amplitude of the displacement response $\widetilde{U}_I$ is determined from Eqs. (10) and (9) with the Fourier transform of the unit impulse $\widetilde{R}_{0I} = 1$

$$\widetilde{U}_I = \frac{1}{\sqrt{\lambda^2 - a_0^2}} \tag{12}$$

The unit-impulse response $\tilde{u}_I(t)$ is equal to the inverse Fourier transform of $\widetilde{U}_I$ (Eq. (12))

$$\tilde{u}_I(t) = \frac{c}{h} J_0\left(\lambda \frac{ct}{h}\right) H(t) \tag{13}$$

where J_0 is the zero order first kind Bessel function, $H(t)$ is the Heaviside-step function ($H(t < 0) = 0$, $H(t \geq 0) = 1$), and $\overline{t} = ct/h$ represents the dimensionless time. At large time ($\overline{t} \gg 1$), the asymptotic solution of the unit-impulse response is expressed as

$$\tilde{u}_I(t) \to \sqrt{\frac{2h}{\pi\lambda ct}} \cos\left(\lambda \frac{ct}{h} - \frac{\pi}{4}\right) \tag{14}$$

It oscillates at a period of $T = 2\pi h/(\lambda c)$. This period corresponds to the dimensionless cut-off frequency $a_0 = \lambda$ where the dynamic stiffness coefficient is equal to zero. The unit-impulse response exhibits a long-lasting oscillation with a very slow decay rate of $\sqrt{T/t}$ (see Fig. 10 in Section 5).

The displacement response to a prescribed traction $\tilde{\tau}_0(t)$ is expressed as a convolution integral

$$\tilde{u}(t) = \frac{c}{h} \int_0^t J_0\left(\lambda \frac{c(t-\tau)}{h}\right) \tilde{\tau}_0(\tau) \mathrm{d}\tau \tag{15}$$

2.2 Equation of dynamic stiffness coefficient

An equation of the dynamic stiffness coefficient is derived from the wave equation and the definition of the dynamic stiffness coefficient. Eliminating the force amplitude $\widetilde{R}$ from Eqs. (7) and (9) leads to

$$h\frac{\mathrm{d}\widetilde{U}}{\mathrm{d}x} = -S\widetilde{U} \tag{16}$$

Differentiating Eq. (16) with respect to x and multiplying the result by h yield

$$h^2\frac{\mathrm{d}^2\widetilde{U}}{\mathrm{d}x^2} = -Sh\frac{\mathrm{d}\widetilde{U}}{\mathrm{d}x} - h\frac{\mathrm{d}S}{\mathrm{d}x}\widetilde{U} = \left(S^2 - h\frac{\mathrm{d}S}{\mathrm{d}x}\right)\widetilde{U} \tag{17}$$

Substituting Eq. (17) into Eq. (4) multiplied by h^2 results, for an arbitrary $\widetilde{U}$, in

$$S^2 - \frac{\mathrm{d}S}{\mathrm{d}x} + a_0^2 - \lambda^2 = 0 \tag{18}$$

As both a_0 (Eq. (5)) and the eigenvalue λ are independent of x, the dynamic stiffness coefficient is a function of a_0 only, i.e., $\mathrm{d}S/\mathrm{d}x = 0$. Equation (18) is, therefore, rewritten as

$$(S(a_0))^2 + a_0^2 - \lambda^2 = 0 \tag{19}$$

which is an algebraic equation. Its positive solution is given in Eq. (10).

3 DOUBLY-ASYMPTOTIC CONTINUED FRACTION SOLUTION FOR DYNAMIC STIFFNESS

A continued fraction solution for the dynamic stiffness coefficient can be obtained recursively as a singly-asymptotic solution at the high-frequency limit ($\omega \to +\infty$) as derived in Reference [40]. However, in the case of semi-infinite layer, it does not converge at all when the frequency is below the cut-off frequency as will be demonstrated in Section 5.

In order to improve the behavior of the singly-asymptotic solution, a doubly-asymptotic continued fraction solution is thus developed. After the high-frequency continued fraction solution is determined as in Reference [40], the differential equation of the residual term is solved again as a continued fraction, but the constants are determined at the low-frequency limit ($\omega \to 0$) instead.

3.1 High-frequency continued fraction

The construction of the high-frequency continued fraction solution for Eq. (19) follows the procedure in Reference [40]. In this particular case, an order M_H continued fraction solution is expressed as

$$S(a_0) = (\mathrm{i}a_0)C_\infty - \cfrac{\lambda^2}{(\mathrm{i}a_0)Y_1^{(1)} - \cfrac{\lambda^2}{(\mathrm{i}a_0)Y_1^{(2)} - \cfrac{\lambda^2}{\cdots - \cfrac{\lambda^2}{(\mathrm{i}a_0)Y_1^{(M_H)} - \cfrac{\lambda^2}{Y^{(M_H+1)}(a_0)}}}}} \tag{20}$$

where the constants C_∞ and $Y_1^{(i)}$ ($i = 1, 2, \ldots, M_H$) are determined by satisfying Eq. (19) at the high-frequency limit ($a_0 \to +\infty$). The negative sign in front of each term is selected intentionally so that the open boundary can be easily expressed with symmetric coefficient matrices (see Section 4). Equation (20) is equivalent to

$$S(a_0) = (\mathrm{i}a_0)C_\infty - \lambda^2 (Y^{(1)}(a_0))^{-1} \tag{21a}$$

$$Y^{(i)}(a_0) = (\mathrm{i}a_0)Y_1^{(i)} - \lambda^2 (Y^{(i+1)}(a_0))^{-1} \qquad (i = 1, 2, \ldots, M_H) \tag{21b}$$

where $Y^{(1)}(a_0)$ is of the order $(\mathrm{i}a_0)^{-1}$ as $a_0 \to +\infty$. When a singly-asymptotic solution is considered, the residual term $\lambda^2 (Y^{(M_H+1)}(a_0))^{-1}$ is neglected.

Substituting Eq. (21a) into Eq. (19) results in an equation in terms of a power series of $(\mathrm{i}a_0)$

$$(\mathrm{i}a_0)^2 \left(C_\infty^2 - 1\right) + \lambda^2 \left(-1 - 2(\mathrm{i}a_0)C_\infty (Y^{(1)}(a_0))^{-1} + \lambda^2 (Y^{(1)}(a_0))^{-2}\right) = 0 \tag{22}$$

This equation is satisfied by setting, in descending order, the two terms to zero. The first term is an equation for damping coefficient C_∞. To satisfy the radiation condition, the positive solution is chosen

$$C_\infty = 1 \tag{23}$$

The second term of Eq. (22) is an equation of $Y^{(1)}(a_0)$ as C_∞ is known (Eq. (23)). To derive a recursive formula for determining the constants of the continued fraction, it is rewritten as the $i = 1$ case of

$$\lambda^2 - 2b_1^{(i)}(\mathrm{i}a_0)Y^{(i)}(a_0) - (Y^{(i)}(a_0))^2 = 0 \tag{24}$$

with the constant

$$b_1^{(1)} = 1 \tag{25}$$

Substituting Eq. (21b) into Eq. (24) leads to an equation in terms of a power series of $(\mathrm{i}a_0)$

$$-(\mathrm{i}a_0)^2\left((Y_1^{(i)})^2 + 2b_1^{(i)}Y_1^{(i)}\right) + \lambda^2\left(1 + 2(\mathrm{i}a_0)(Y_1^{(i)} + b_1^{(i)})(Y^{(i+1)}(a_0))^{-1} - \lambda^2(Y^{(i+1)}(a_0))^{-2}\right) = 0 \tag{26}$$

Again, this equation is satisfied by setting the two terms to zero. The non-zero solution of the $(\mathrm{i}a_0)^2$ term is equal to

$$Y_1^{(i)} = -2b_1^{(i)} \tag{27}$$

By using the solution of $Y_1^{(i)}$ in Eq. (27), the second term of Eq. (26) is rearranged as

$$\lambda^2 + 2b_1^{(i)}(\mathrm{i}a_0)Y^{(i+1)}(a_0) - (Y^{(i+1)}(a_0))^2 = 0 \tag{28}$$

Introducing the recursive formula for updating the constant

$$b_1^{(i+1)} = -b_1^{(i)} \tag{29}$$

Equation (28) is simply the $(i+1)$ case of Eq. (24). From Eqs. (25) and (29),

$$b_1^{(i)} = (-1)^{i+1} \tag{30}$$

applies. $Y_1^{(i)}$ is obtained explicitly from Eq. (27) as

$$Y_1^{(i)} = (-1)^i 2 \tag{31}$$

The high-frequency continued fraction solution in Eq. (20) (or Eq. (21)) is constructed from the solutions of the constants C_∞ in Eq. (23) and $Y_1^{(i)}$ in Eq. (31). For example, Eq. (20) is expressed for the order $M_H = 2$ high-frequency continued fraction as

$$S(a_0) = (\mathrm{i}a_0) - \cfrac{\lambda^2}{-2(\mathrm{i}a_0) - \cfrac{\lambda^2}{2(\mathrm{i}a_0) - \cfrac{\lambda^2}{Y^{(3)}(a_0)}}} \tag{32}$$

3.2 Link with other open boundaries for plane waves

The singly-asymptotic continued fraction solution in Eq. (20) is expressed by using Eqs. (23) and (31) as

$$\frac{S(a_0)}{(\mathrm{i}a_0)} = 1 - \cfrac{(\lambda/(\mathrm{i}a_0))^2}{-2 - \cfrac{(\lambda/(\mathrm{i}a_0))^2}{2 - \cfrac{(\lambda/(\mathrm{i}a_0))^2}{-2-\ldots}}} = 1 + \cfrac{(\lambda/(\mathrm{i}a_0))^2}{2 + \cfrac{(\lambda/(\mathrm{i}a_0))^2}{2 + \cfrac{(\lambda/(\mathrm{i}a_0))^2}{2+\ldots}}} = 1 - \cfrac{(\lambda/a_0)^2}{2 - \cfrac{(\lambda/a_0)^2}{2 - \cfrac{(\lambda/a_0)^2}{2-\ldots}}} \tag{33}$$

Several open boundaries have been constructed based on the continued fractions of the function $\sqrt{1+x}$, where x may represent the wave number, pseudo-differential operator or the angle of incidence of a plane wave depending on the particular formulation. For example, the third approximation expressed in Eq. 1.13 of Reference [42] is based on the continued fraction

$$\sqrt{1+x} = 1 + \cfrac{x}{2 + \cfrac{x}{2}} \tag{34}$$

When $x = (\lambda/\mathrm{i}a_0)^2 = -(\lambda/a_0)^2$ is assumed, Eq. (34) is equivalent to the second order singly-asymptotic continued fraction in Eq. (33).

It has been shown in Reference [30] that, when all the angles of ideal transmission are selected as 0, the multi-directional open boundary proposed by Higdon [43] corresponds to the continued fraction of $\cos\theta = \sqrt{1-\sin^2\theta}$ (Eq. 15 [30])

$$\cos\theta = 1 - \cfrac{\sin^2\theta}{2 - \cfrac{\sin^2\theta}{2 - \cfrac{\sin^2\theta}{2-\ldots}}} \tag{35}$$

where θ is the angle of incidence (the angle between the direction of propagation of a plane wave and the outward normal of the boundary). Equation (35) is equivalent to Eq. (34) for the same order of continued fraction when $x = -\sin^2\theta$ is assumed. By comparing Eq. (33) to Eq. (35), it can be identified that the two equations are identical when setting

$$\sin\theta = \lambda/a_0 \tag{36}$$

Equation (36) relates the dimensionless frequency a_0 to the angle of incidence θ.

As $\sin\theta$ is bounded between 0 and 1, the performance of open boundaries based on this continued fraction is controlled for $a_0 \geq \lambda$, i.e. above the cut-off frequency, only. Their accuracy below the cut-off frequency ($a_0 < \lambda$), i.e. for the evanescent waves, is not guaranteed. This is illustrated in Fig. 2 by comparing the continued fraction solution with the exact solution (Eq. (10)). The dynamic stiffness coefficient and the dimensionless frequency are normalized as expressed in Eq. (11). When the frequency is slightly above the cut-off frequency ($a_0/\lambda > 1.25$), the order $M_H = 2$ continued fraction solution is already very accurate. However, the error below the cut-off frequency is very large. The imaginary part exhibits a discontinuous point. The real part of the continued fraction solution is always equal to zero independent of the order as expected from Eq. (32). As the order of the continued fraction increases to $M_H = 5$ and $M_H = 11$, the accuracy of the results at frequencies immediately above the cut-off frequency

improves. The result of $M_H = 11$ is indistinguishable from the exact solution above the cut-off frequency. Below the cut-off frequency, the number of discontinuous points in the imaginary part increases and the accuracy does not improve. The error at the low-frequency range affects the accuracy of late-time response in the time domain as illustrated numerically in Section 5.

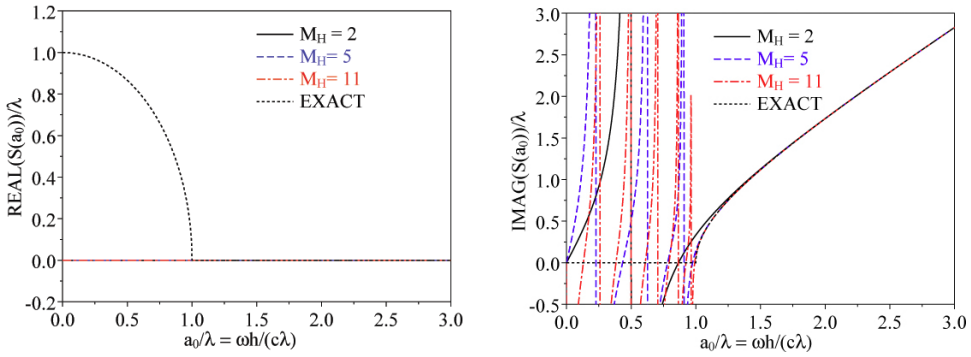

Figure 2: High-frequency continued fraction solution for dynamic stiffness coefficient of semi-infinite layer

A reflection coefficient based on the angles of incidence of propagating plane waves is often derived in the literature to evaluate the performance of an open boundary. It is meaningful for only $0 \leq \sin\theta \leq 1$, i.e., the frequency range $a_0 \geq \lambda$. As the order increases, the reflection coefficient becomes smaller but the accuracy below the cut-off frequency does not necessarily improve. This is consistent with the statement in Reference [34] that: "a comparison of boundary conditions based solely on the magnitude of reflection coefficients for propagating modes is a poor predictor of actual performance, particularly as the order is increased".

3.3 Doubly-asymptotic continued fraction

The procedure in Section 3.1 leads to not only a high-frequency continued fraction solution for the dynamic stiffness coefficient but also an equation of the residual term $Y^{(M_H+1)}(a_0)$, i.e., the $i = M_H + 1$ case of Eq. (24) with the constant $b_1^{(M_H+1)}$ given in Eq. (30). To determine a solution that is valid over the whole frequency range, a low-frequency continued fraction solution for the residual term $Y^{(M_H+1)}(a_0)$ is sought.

Denoting the residual term as

$$Y_L(a_0) = Y^{(M_H+1)}(a_0) \tag{37}$$

the $i = M_H + 1$ case of Eq. (24) is expressed as

$$\lambda^2 - 2b_L(\mathrm{i}a_0)Y_L(a_0) - (Y_L(a_0))^2 = 0 \tag{38}$$

with the constant

$$b_L = b_1^{(M_H+1)} = (-1)^{M_H} \tag{39}$$

given in Eq. (30). The continued fraction solution for $Y_L(a_0)$ at the low-frequency limit is

written as

$$Y_L(a_0) = Y_{L0}^{(0)} + (\mathrm{i}a_0)Y_{L1}^{(0)} - \cfrac{(\mathrm{i}a_0)^2}{Y_{L0}^{(1)} - \cfrac{(\mathrm{i}a_0)^2}{Y_{L0}^{(2)} - \cfrac{(\mathrm{i}a_0)^2}{\cdots - \cfrac{(\mathrm{i}a_0)^2}{Y_{L0}^{(M_L)}}}}} \tag{40}$$

It is equivalent to

$$Y_L(a_0) = Y_{L0}^{(0)} + (\mathrm{i}a_0)Y_{L1}^{(0)} - (\mathrm{i}a_0)^2(Y_L^{(1)}(a_0))^{-1} \tag{41a}$$

$$Y_L^{(i)}(a_0) = Y_{L0}^{(i)} - (\mathrm{i}a_0)^2(Y_L^{(i+1)}(a_0))^{-1} \qquad (i = 1, 2, \ldots, M_L) \tag{41b}$$

where the constant term in Eq. (41b) is omitted as its solution is equal to zero. For an M_L order continued fraction, the residual $(\mathrm{i}a_0)^2/Y_L^{(i+1)}(a_0)$ is neglected. The constants $Y_{L0}^{(i)}$ ($i = 1, 2, \cdots, M_L$) and $Y_{L1}^{(0)}$ are determined by satisfying Eq. (38) at the low-frequency limit ($a_0 \to 0$).

Substituting Eq. (41a) into Eq. (38) leads to an equation in terms of a power series of $(\mathrm{i}a_0)$

$$\begin{aligned}\left(\lambda^2 - (Y_{L0}^{(0)})^2\right) - (\mathrm{i}a_0)\left(2b_L Y_{L0}^{(0)} + 2Y_{L0}^{(0)}Y_{L1}^{(0)}\right) + (\mathrm{i}a_0)^2\Big(-2b_L Y_{L1}^{(0)} - (Y_{L1}^{(0)})^2 \\ +2(Y_{L0}^{(0)} + (\mathrm{i}a_0)(Y_{L1}^{(0)} + b_L))(Y_L^{(1)}(a_0))^{-1} - (\mathrm{i}a_0)^2(Y_L^{(1)}(a_0))^{-2}\Big) = 0\end{aligned} \tag{42}$$

As the low-frequency solution is being sought, Eq. (42) is satisfied by setting the coefficients of the power series to zero in ascending order. Setting the constant term to zero results in

$$\lambda^2 - (Y_{L0}^{(0)})^2 = 0 \tag{43}$$

Out of the two solutions, the one leading to the correct static stiffness $S(a_0 = 0) = \lambda$ should be chosen. Inspecting Eq. (20) with $Y^{(M_H+1)}(a_0 = 0) = Y_L(a_0 = 0) = Y_{L0}^{(0)}$ (Eqs. (37) and (41a)), the solution is

$$Y_{L0}^{(0)} = (-1)^{M_H+1}\lambda \tag{44}$$

Setting the coefficient of the $(\mathrm{i}a_0)$ term in Eq. (42) to zero leads to an equation for $Y_{L1}^{(0)}$. By using Eq. (39), its solution is expressed as

$$Y_{L1}^{(0)} = -b_L = (-1)^{M_H+1} \tag{45}$$

Setting the coefficient of the $(\mathrm{i}a_0)^2$ term in Eq. (42) to zero yields an equation of $Y_L^{(1)}(a_0)$. After substituting the solutions for $Y_{L0}^{(0)}$ (Eq. (44)) and $Y_{L1}^{(0)}$ (Eq. (45)), the equation is expressed as the $i = 1$ case of the following equation:

$$(\mathrm{i}a_0)^2 - 2b_L^{(i)}Y_L^{(i)}(a_0) - (Y_L^{(i)}(a_0))^2 = 0 \tag{46}$$

with the constant (Eq. (39))

$$b_L^{(1)} = -b_L\lambda = (-1)^{M_H+1}\lambda \tag{47}$$

A recursive procedure for determining the constants $Y_{L0}^{(i)}$ in Eq. (41b) is established by substituting Eq. (41b) into Eq. (46). The resulting expression is arranged as

$$-\left(2b_L^{(i)}Y_{L0}^{(i)}+(Y_{L0}^{(i)})^2\right)+(\mathrm{i}a_0)^2\left(1+2(b_L^{(i)}+Y_{L0}^{(i)})(Y_L^{(i+1)}(a_0))^{-1} -(\mathrm{i}a_0)^2(Y_L^{(i+1)}(a_0))^{-2}\right)=0 \quad (48)$$

Setting the term independent of $(\mathrm{i}a_0)$ to zero yields an equation for $Y_{L0}^{(i)}$. Its non-zero solution is

$$Y_{L0}^{(i)}=-2b_L^{(i)} \quad (49)$$

Setting the $(\mathrm{i}a_0)^2$ term to zero and using Eq. (49) result in the equation of $Y_L^{(i+1)}(a_0)$

$$(\mathrm{i}a_0)^2+2b_L^{(i)}Y_L^{(i+1)}(a_0)-(Y_L^{(i+1)}(a_0))^2=0 \quad (50)$$

It is simply the $(i+1)$ case of Eq. (46) with the constant

$$b_L^{(i+1)}=-b_L^{(i)} \quad (51)$$

Equations (47) and (51) lead to

$$b_L^{(i)}=(-1)^{M_H+i}\lambda \qquad i=1,2,\ldots M_L \quad (52)$$

The constants of the continued fraction are expressed explicitly as

$$Y_{L0}^{(i)}=(-1)^{M_H+i+1}2\lambda \qquad i=1,2,\ldots M_L \quad (53)$$

As an example, the order $M_L=2$ low-frequency continued fraction for the residual $Y^{(3)}(a_0)$ of the order $M_H=2$ high-frequency continued fraction solution is expressed as

$$Y^{(3)}(a_0)=Y_L(a_0)=-\lambda-(\mathrm{i}a_0)-\cfrac{(\mathrm{i}a_0)^2}{2\lambda-\cfrac{(\mathrm{i}a_0)^2}{-2\lambda}} \quad (54)$$

The doubly-asymptotic continued fraction solution is constructed by combining the high-frequency continued fraction solution in Eq. (20) (or Eq. (21)) with the low-frequency solution in Eq. (40) (or Eq. (41)) using $Y^{(M_H+1)}(a_0)=Y_L(a_0)$ (Eq. (37)). For example, the order $M_H=M_L=2$ doubly-asymptotic continued fraction solution is obtained from Eqs. (32) and (54) as

$$S(a_0)=(\mathrm{i}a_0)-\cfrac{\lambda^2}{-2(\mathrm{i}a_0)-\cfrac{\lambda^2}{2(\mathrm{i}a_0)-\cfrac{\lambda^2}{-\lambda-(\mathrm{i}a_0)-\cfrac{(\mathrm{i}a_0)^2}{2\lambda-\cfrac{(\mathrm{i}a_0)^2}{-2\lambda}}}}} \quad (55)$$

The real and imaginary parts of the order $M_H=M_L=2$ doubly-asymptotic solution are compared with the exact solution in Fig. 3. The present result is very accurate outside of a small range around the cut-off frequency.

Further evaluation of the accuracy of the doubly-asymptotic solution is reported in Section 5.

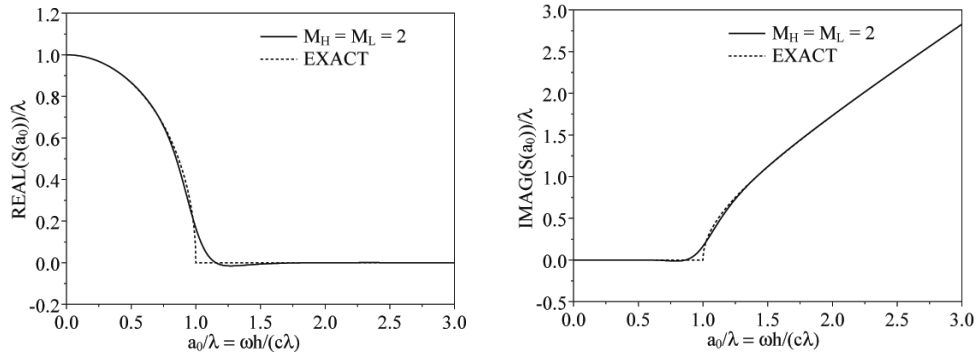

Figure 3: Doubly-asymptotic continued fraction solution for dynamic stiffness coefficient of semi-finite layer: $M_H = M_L = 2$

4 IMPLEMENTATION OF CONTINUED FRACTION SOLUTION IN THE TIME DOMAIN

In the frequency domain, the open boundary condition is expressed as the force-displacement relationship (Eq. (9))

$$\widetilde{R} = S(a_0)\widetilde{U} \tag{56}$$

When the dynamic stiffness coefficient $S(a_0)$ is expressed as a continued fraction solution, the force-displacement relationship can be formulated in the time domain as a system of first-order ordinary differential equations with time-independent coefficient matrices, which represents a temporally local open boundary.

A doubly-asymptotic continued fraction solution which includes the expressions of the semi-infinite layer as special case is considered

$$S(a_0) = K_\infty + (\mathrm{i}a_0)C_\infty - m^2(Y^{(1)}(a_0))^{-1} \tag{57a}$$

$$Y^{(i)}(a_0) = Y_0^{(i)} + (\mathrm{i}a_0)Y_1^{(i)} - m^2(Y^{(i+1)}(a_0))^{-1} \qquad (i = 1, 2, \ldots, M_H) \tag{57b}$$

$$Y_L(a_0) = Y^{(M_H+1)}(a_0) \tag{57c}$$

$$Y_L(a_0) = Y_{L0} + (\mathrm{i}a_0)Y_{L1} - (\mathrm{i}a_0)^2(Y_L^{(1)}(a_0))^{-1} \tag{57d}$$

$$Y_L^{(i)}(a_0) = Y_{L0}^{(i)} + (\mathrm{i}a_0)Y_{L1}^{(i)} - (\mathrm{i}a_0)^2(Y_L^{(i+1)}(a_0))^{-1} \qquad (i = 1, 2, \ldots, M_L) \tag{57e}$$

with the dimensionless frequency

$$a_0 = \frac{\omega r_0}{c} \tag{58}$$

Note that in Eqs. (21) and (41), $K_\infty = Y_0^{(i)} = Y_{L1}^{(i)} = 0$ and $m = \lambda$ applies, and the characteristic length r_0 in Eq. (58) must be replaced with the depth h of the layer. Substituting Eq. (57a) into the force-displacement relationship in Eq. (56) leads to

$$\widetilde{R} = S(a_0)\widetilde{U} = K_\infty\widetilde{U} + (\mathrm{i}a_0)C_\infty\widetilde{U} - m\widetilde{U}^{(1)} \tag{59}$$

where the auxiliary variable $\widetilde{U}^{(1)}$ is defined as

$$\widetilde{U}^{(1)} = m(Y^{(1)}(a_0))^{-1}\widetilde{U} \tag{60}$$

and then reformulated as

$$m\widetilde{U} = Y^{(1)}(a_0)\widetilde{U}^{(1)} \tag{61}$$

which is in the same form as the force-displacement relationship (Eq. (56)). Similarly, an auxiliary variable is introduced for each term of the continued fraction in Eq. (57b)

$$m\widetilde{U}^{(i)} = Y^{(i+1)}(a_0)\widetilde{U}^{(i+1)} \qquad (i = 0, 1, 2, \ldots, M_H) \tag{62}$$

where Eq. (61) is included as the $i = 0$ case with $\widetilde{U}^{(0)} = \widetilde{U}$. Multiplying Eq. (57b) by $\widetilde{U}^{(i)}$ and using the definition of auxiliary variables in Eq. (62) formulated at i and $i-1$ result in

$$m\widetilde{U}^{(i-1)} = Y_0^{(i)}\widetilde{U}^{(i)} + (\mathrm{i}a_0)Y_1^{(i)}\widetilde{U}^{(i)} - m\widetilde{U}^{(i+1)} \qquad (i = 1, 2, \ldots, M_H) \tag{63}$$

The residual $\widetilde{U}^{(M_H+1)}$ of an order M_H high-frequency continued fraction solution is expressed in Eq. (62) at $i = M_H$ as

$$m\widetilde{U}^{(M_H)} = Y^{(M_H+1)}(a_0)\widetilde{U}^{(M_H+1)} \tag{64}$$

$Y^{(M_H+1)} = Y_L(a_0)$ (Eq. (57c)) is expressed in Eq. (57d) as a low-frequency continued fraction solution. Multiplying Eq. (57d) by $\widetilde{U}^{(M_H+1)}$ and using Eqs. (57c) and (64) lead to

$$m\widetilde{U}^{(M_H)} = Y_{L0}\widetilde{U}^{(M_H+1)} + (\mathrm{i}a_0)Y_{L1}\widetilde{U}^{(M_H+1)} - (\mathrm{i}a_0)\widetilde{U}_L^{(1)} \tag{65}$$

where the auxiliary variable $\widetilde{U}_L^{(1)}$ is defined in

$$(\mathrm{i}a_0)\widetilde{U}^{(M_H+1)} = Y_L^{(1)}(a_0)\widetilde{U}_L^{(1)} \tag{66}$$

Again, an auxiliary variable is introduced for each term of the continued fraction in Eq. (57e) as

$$(\mathrm{i}a_0)\widetilde{U}_L^{(i)} = Y_L^{(i+1)}(a_0)\widetilde{U}_L^{(i+1)} \qquad (i = 0, 1, 2, \ldots, M_L) \tag{67}$$

with $\widetilde{U}_L^{(0)} = \widetilde{U}^{(M_H+1)}$. Multiplying Eq. (57e) by $\widetilde{U}_L^{(i)}$ and using Eq. (67) at $i-1$ and i yield

$$(\mathrm{i}a_0)\widetilde{U}_L^{(i-1)} = Y_{L0}^{(i)}\widetilde{U}_L^{(i)} + (\mathrm{i}a_0)Y_{L1}^{(i)}\widetilde{U}_L^{(i)} - (\mathrm{i}a_0)\widetilde{U}_L^{(i+1)} \qquad (i = 1, 2, \ldots, M_L) \tag{68}$$

For the order M_L low-frequency solution, the approximation $\widetilde{U}_L^{(M_L+1)} = 0$ is introduced.

Equations (59), (63), (65) and (68) are all combined to form a matrix equation

$$([K_h] + \mathrm{i}\omega[C_h])\{Z\} = \{F\} \tag{69}$$

with

$$\{Z\} = [\widetilde{U}, \widetilde{U}^{(1)}, \cdots, \widetilde{U}^{(M_H)}, \widetilde{U}^{(M_H+1)}, \widetilde{U}_L^{(1)}, \cdots, \widetilde{U}_L^{(M_L)}]^T \tag{70a}$$

$$\{F\} = [\widetilde{R}, 0, \cdots, 0, 0, 0, \cdots, 0]^T \tag{70b}$$

$$[K_h] = \begin{bmatrix} K_\infty & -m & & & & & & \\ -m & Y_0^{(1)} & \ddots & & & & & \\ & \ddots & \ddots & -m & & & & \\ & & -m & Y_0^{(M_H)} & -m & & & \\ & & & -m & Y_{L0} & 0 & & \\ & & & & 0 & Y_{L0}^{(1)} & \ddots & \\ & & & & & \ddots & \ddots & 0 \\ & & & & & & 0 & Y_{L0}^{(M_L)} \end{bmatrix} \tag{70c}$$

$$[C_h] = \frac{h}{c} \begin{bmatrix} C_\infty & 0 & & & & & & \\ 0 & Y_1^{(1)} & \ddots & & & & & \\ & \ddots & \ddots & 0 & & & & \\ & & 0 & Y_1^{(M_H)} & 0 & & & \\ & & & 0 & Y_{L1} & -1 & & \\ & & & & -1 & Y_{L1}^{(1)} & \ddots & \\ & & & & & \ddots & \ddots & -1 \\ & & & & & & -1 & Y_{L1}^{(M_L)} \end{bmatrix} \tag{70d}$$

The function $\{Z\}$ includes the displacement amplitude on the boundary and all the auxiliary variables, and the only non-zero entry at the right-hand side $\{F\}$ is the excitation force $\widetilde{R}$ on the boundary. Note that Eq. (58) is substituted into the equation to replace $\mathrm{i}a_0$ with $\mathrm{i}\omega$. The time-independent matrices $[K_h]$ and $[C_h]$ are tri-diagonal and symmetric. Equation (69) is expressed in the time domain as

$$[K_h]\{z(t)\} + [C_h]\{\dot{z}(t)\} = \{f(t)\} \tag{71}$$

It represents a temporally local high-order open boundary applicable to one mode of wave propagation in a semi-infinite layer with a constant depth.

5 NUMERICAL EXAMPLES

The accuracy of the proposed doubly-asymptotic open boundary is evaluated in this section. Newmark's method with $\gamma = 0.5$ and $\beta = 0.25$ (average acceleration scheme) is employed for the time integration. The size of the time step is chosen as $\Delta t = 0.01h/(\lambda c)$ for the semi-infinite layer.

When the present doubly-asymptotic open boundary is employed, the only two parameters that the users must select are the orders of high- and low-frequency continued fractions M_H and M_L. In this paper, the same value is chosen for both parameters. With this simple, although not necessarily optimal, choice, the doubly-asymptotic open boundaries perform much better than the singly-asymptotic open boundaries with the same number of terms do.

The excitation by a unit impulse of traction $\tilde{\tau}_{0I}(t) = \delta(t)$ is chosen to evaluate the accuracy of open boundaries as it covers the whole frequency range. When a unit impulse is applied,

the initial condition is obtained by integrating Eq. (71) with the matrix $[C_h]$ given in Eq. (70d) (Note that the first entry of $\{f(t)\}$ and $\{z(t)\}$ is $\tilde{\tau}_{0I}(t)$ and $\tilde{u}(t)$, respectively.)

$$\tilde{u}(t=0) = c/(hC_\infty) \tag{72}$$

To investigate the performance of the open boundary at a specified frequency range, the surface traction is prescribed as a Ricker wavelet. The time history of the Ricker wavelet is given as

$$\tilde{\tau}_0(t) = A_R \left(1 - 2\left(\frac{t-t_s}{t_0}\right)^2\right) \exp\left(-\left(\frac{t-t_s}{t_0}\right)^2\right) \tag{73}$$

where t_s is the time when the wavelet reaches its maximum, $2/t_0$ is the dominant angular frequency of the wavelet and A_R is the amplitude. The Fourier transform of the wavelet is expressed as

$$\tilde{R}_0(\omega) = 0.5\sqrt{\pi} A_R t_0 (\omega t_0)^2 \mathrm{e}^{-0.25(\omega t_0)^2} \tag{74}$$

A Ricker wavelet with the parameters $\bar{t_s} = ct_s/h = 1$, $\bar{t_0} = ct_0/h = 0.2$ and $A_R = 10$ is shown in Fig. 4(a). The amplitude of its Fourier transform is plotted in Fig. 4(b). The dominant dimensionless frequency of this wavelet is $a_0 = 10$.

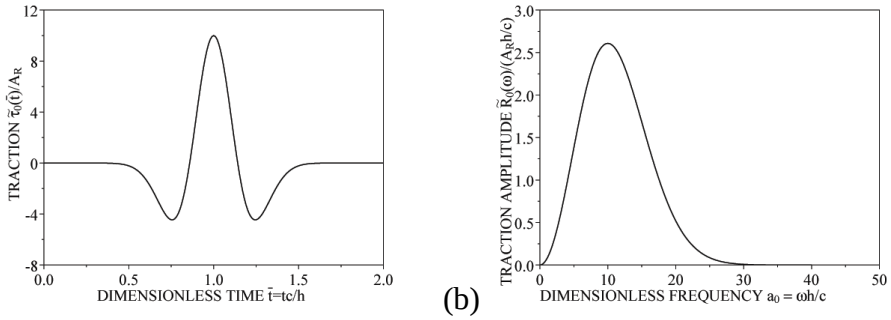

Figure 4: Prescribed traction as a Ricker wavelet: (a) Time history; (b) Fourier transform

The case of a semi-infinite layer with a constant depth is a stringent test due to the existence of a cut-off frequency. Since the dynamic stiffness is not smooth at the cut-off frequency, this case is especially challenging for the doubly-asymptotic continued fraction solution. At the cut-off frequency, the dynamic stiffness is equal to zero. As a result, waves around the cut-off frequency decay at a very slow rate (Eq. (14)). This requires that an open boundary has to be accurate over a large time duration. The investigation of the semi-infinite layer is also significant because the construction of several higher-order open boundaries is related to this case as shown in Section 3.2.

The performance of the singly-asymptotic open boundary based solely on the high-frequency continued fraction solution is evaluated at first. The dynamic stiffness coefficient of the order $M_H = 5$ continued fraction is plotted in Fig. 2. The cut-off frequency exists at $a_0/\lambda = 1$. The large error of the dynamic stiffness coefficient below the cut-off frequency ($a_0/\lambda < 1$) indicates that the high-order singly-asymptotic open boundary is unable to transmit evanescent waves. This is confirmed by the unit-impulse response of the $M_H = 5$ open boundary plotted in Fig. 5. The early-time (high-frequency) response is very accurate. The response after the dimensionless time $\lambda\bar{t} > 10$ suddenly exhibits a very large error and the amplitude of the error does not decay

with time. Since this phenomenon is very similar to fictitious reflections caused by enforcing a simple (free or fixed) boundary condition at a certain distance, it is referred to as "fictitious reflections" in this paper.

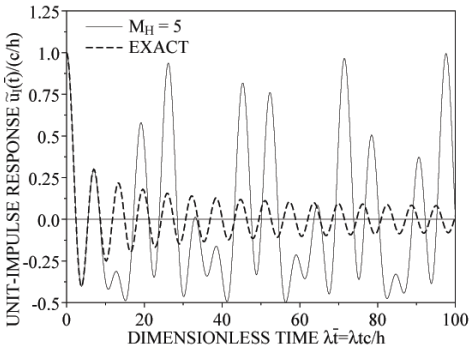

Figure 5: Unit-impulse response of semi-infinite layer by singly-asymptotic boundary: $M_H = 5$

The effect of the order of the singly-asymptotic open boundary on its accuracy is also investigated by considering the orders $M_H = 11$ and $M_H = 99$. The order $M_H = 11$ continued fraction solution has 12 terms (double the number of terms of the $M_H = 5$ solution) while the order $M_H = 99$ continued fraction solution has 100 terms. Above the cut-off frequency, the dynamic stiffness coefficients of both open boundaries are indistinguishable from the exact solution as shown in Fig. 2 (If the dynamic stiffness coefficient of the $M_H = 99$ open boundary is plotted in Fig. 2, the result will be similar to that of the $M_H = 11$ open boundary above the cut-off frequency.). The unit-impulse responses of both open boundaries are shown in Fig. 6. As the order increases, the accuracy improves. However, significant "fictitious reflections" still occur, albeit at later time, even at the order $M_H = 99$. As the amplitude of the "fictitious reflections" does not decay with time, the singly-asymptotic open boundary is unsuitable for the analysis of long-time response.

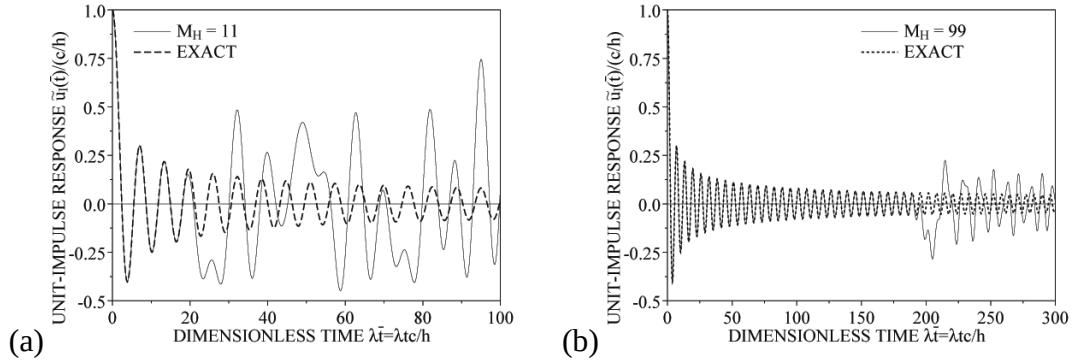

Figure 6: Unit-impulse response of semi-infinite layer by singly-asymptotic boundary: (a) $M_H = 11$; (b) $M_H = 99$

The defect of the singly-asymptotic open boundary in representing low-frequency responses can be mended by employing the doubly-asymptotic continued fraction solution in Section 3.3. The corresponding higher-order doubly asymptotic open boundary is constructed in Section 4. For the $M_H = M_L = 2$ doubly-asymptotic open boundary, of which the dynamic stiffness coefficient is shown in Fig. 3, the unit-impulse response is plotted in Fig. 7. It decays gradually and no "fictitious reflection" appears. It is observed by comparing Fig. 7 with Fig. 5 that the

$M_H = M_L = 2$ open boundary is much more accurate than the $M_H = 5$ open boundary after $\lambda\bar{t} > 10$, although the number of equations of both formulations is equal to 5.

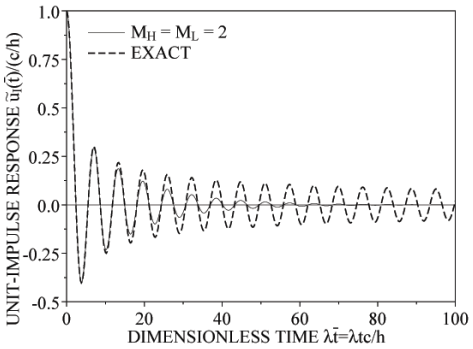

Figure 7: Unit-impulse response of semi-infinite layer by doubly-asymptotic boundary: $M_H = M_L = 2$

The accuracy of the doubly-asymptotic open boundary improves rapidly as its order increases. This is demonstrated by using the order $M_H = M_L = 5$ open boundary. Its dynamic stiffness coefficient is plotted in Fig. 8. It is indistinguishable from the exact solution except for the slight difference close to the cut-off frequency. The unit-impulse response is shown in Fig. 9. Good agreement with the exact solution is observed for about the first 10 periods. Compared with the unit-impulse response of the $M_H = 11$ open boundary, which has the same number of variables, in Fig. 6(a), the doubly-asymptotic open boundary is significantly more accurate at late time. No "fictitious reflection" occurs.

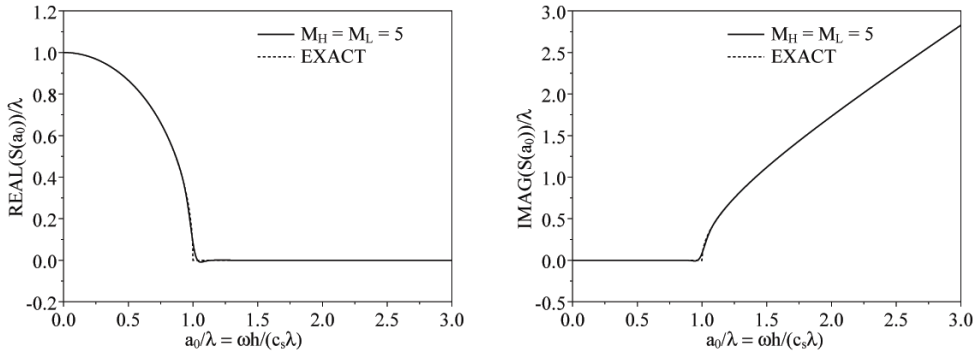

Figure 8: Doubly-asymptotic continued fraction solution for dynamic stiffness coefficient of semi-infinite layer: $M_H = M_L = 5$

To further investigate the convergence of the doubly-asymptotic open boundary, a long-time analysis, with a duration of $\lambda tc/h = 200\pi$, of the unit-impulse response is performed. As the period of the asymptotic solution of the unit-impulse response is $\lambda tc/h = 2\pi$, this duration corresponds to 100 periods of vibration. The amplitude of the unit-impulse response decays from 1 at $t = 0$ to about 0.032. The result of the $M_H = M_L = 24$ open boundary is plotted in Fig. 10(a). The unit-impulse response decays gradually and no "fictitious reflections" occur. The numerical result is indistinguishable from the exact solution at the early stage (Fig. 10(b)) and in the middle of the duration (Fig. 10(c)). At the end of the duration, the error is merely about 0.0015. Thus, the $M_H = M_L = 24$ open boundary is sufficiently accurate for most engineering applications.

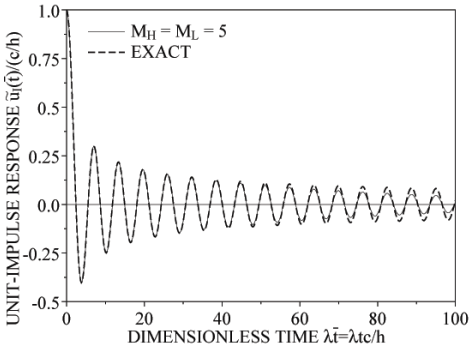

Figure 9: Unit-impulse response of semi-infinite layer by doubly-asymptotic boundary: $M_H = M_L = 5$

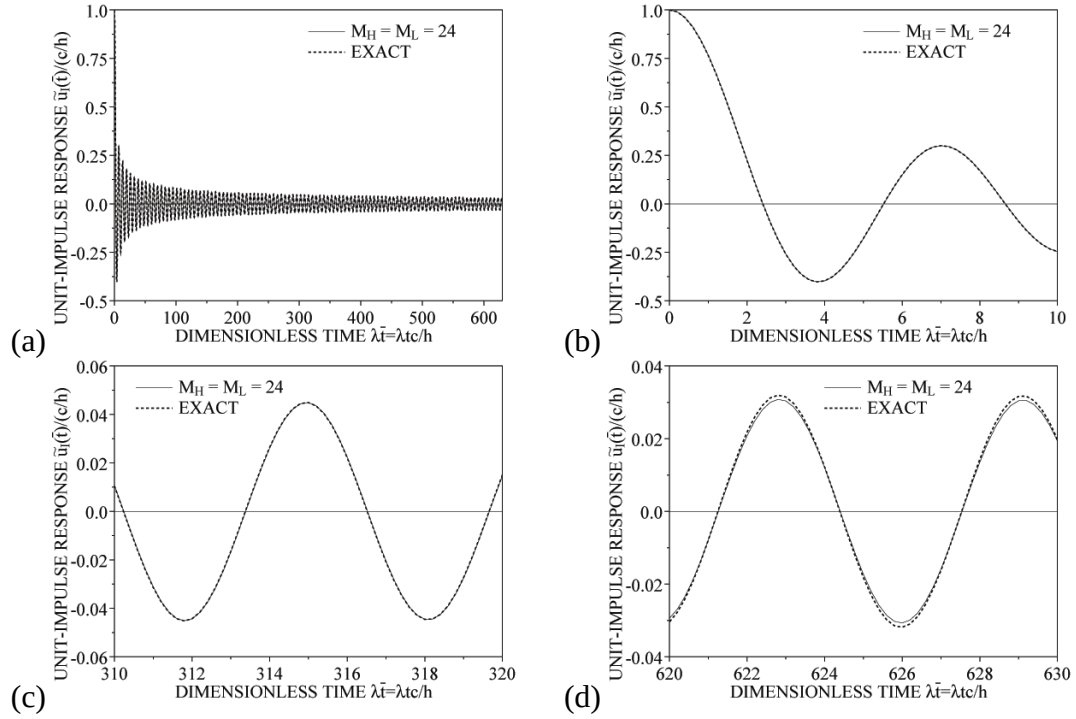

Figure 10: Unit-impulse response of semi-infinite layer by doubly-asymptotic boundary: $M_H = M_L = 24$

The response to a surface traction prescribed as the Ricker wavelet shown in Fig. 4 ($\bar{t_s} = ct_s/h = 1$, $\bar{t_0} = ct_0/h = 0.2$) is computed for three modes $\lambda = 5$, 10 and 15. It is similar to the analysis of the semi-infinite layer by using modal superposition. The same amplitude of surface traction $A_R = 10$ is assumed for all the three modes. The ratios of the dominate dimensionless frequencies to the modal eigenvalues are $a_0/\lambda = 2$, 1 and $2/3$, respectively. The responses of the $M_H = M_L = 24$ doubly-asymptotic open boundary are plotted in Fig. 11. Very good agreement is observed for all the three modes. For comparison, the responses of the $M_H = 99$ singly-asymptotic open boundary are also shown. As its dynamic stiffness coefficient is very accurate above the cut-off frequency ($a_0 > \lambda$), the response for the mode $\lambda = 5$ (the ratio $a_0/\lambda = 2$) is very accurate (Fig. 11(a)) with only a small error after $\bar{t} > 45$. As the mode increases, the "fictitious reflections" appear. For the mode $\lambda = 15$ (the ratio $a_0/\lambda = 0.5$), the amplitude of the "fictitious reflections" is very large. In addition, the "fictitious reflections" arrive earlier as the modal eigenvalue increases.

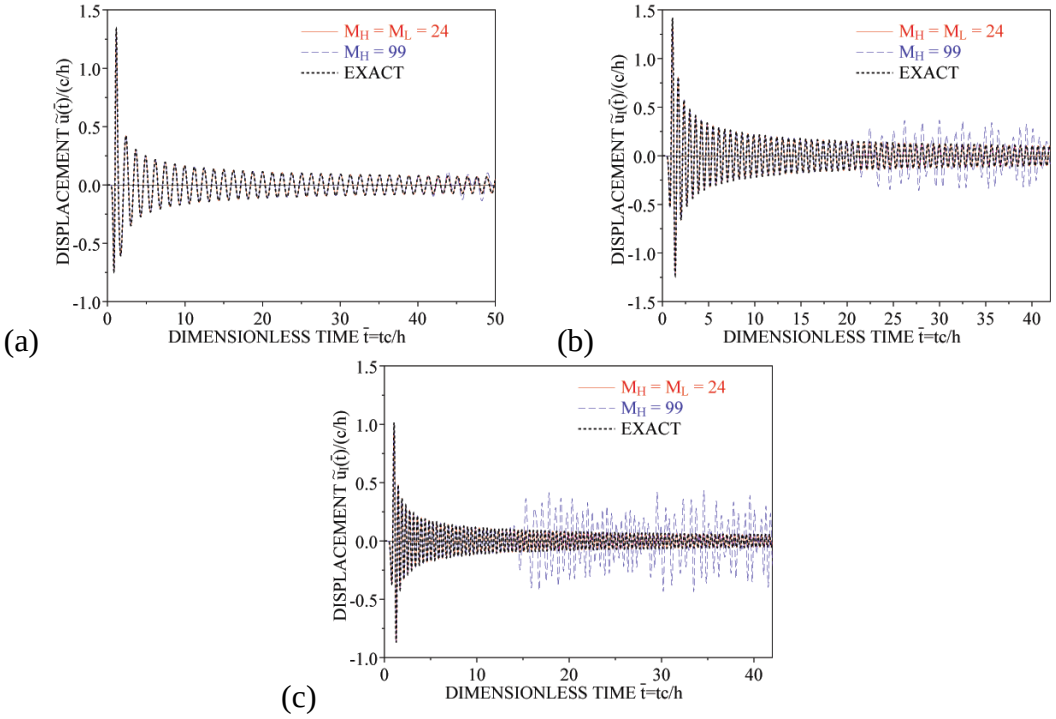

Figure 11: Response of semi-infinite layer to traction varying as Ricker wavelets by $M_H = M_L = 24$ doubly-asymptotic boundary: (a) $\lambda = 5$; (b) $\lambda = 10$; (c) $\lambda = 15$

6 CONCLUSIONS

A novel approach to constructing the high-order doubly asymptotic open boundary of a semi-infinite layer with a constant depth has been proposed. The derivation and implementation have also been presented for the transient analysis of scalar waves propagating in a waveguide. It is found from theoretical formulations and numerical experiments that

1. When a high-order open boundary is based solely on a high-frequency continued fraction expansion of the dynamic stiffness, i.e. singly-asymptotic, it is equivalent to several well-established high-order open boundaries. A singly-asymptotic open boundary condition performs satisfactorily when the dimensionless frequency (ia_0) content of the excitation is mostly higher than the highest modal eigenvalue (λ). However, it is unable to model evanescent waves caused by the part of excitation having dimensionless frequency lower than the highest modal eigenvalue. In a long-time analysis, the error in modeling evanescent waves with the application of the singly-asymptotic open boundary condition appears as numerical pollution similar to the "fictitious reflections" caused by simple boundary conditions.

2. The dynamic stiffness of a doubly-asymptotic open boundary condition converges rapidly to the exact solution in the frequency domain as its order increases. The doubly-asymptotic open boundary condition is able to simulate evanescent waves and the late-time (low-frequency) responses of the semi-infinite layer accurately. This shows a significant improvement in accuracy of the doubly-asymptotic open boundary condition in comparison with the singly-asymptotic open boundary condition with the same number of terms.

3. The high-order doubly asymptotic open boundary condition is expressed as a system of first-order ordinary differential equations in time. The two time-independent coeffi-

cient matrices, the static stiffness and damping matrices, are symmetric and tri-diagonal. Well-established time-stepping schemes in structural dynamics are directly applicable. The amount of computer time and storage are the same as those required by the singly-asymptotic open boundary condition of the same order.

REFERENCES

[1] Luco JE. Linear soil-structure interaction: a review. *Earthquake Ground Motion and Its Effects on Structures, AMD(Ed. S.K. Datta), ASME* 1982; **53**: 41–57.

[2] Kausel E. Local transmitting boundaries. *Journal of Engineering Mechanics, ASCE* 1988; **114**: 1011–1027.

[3] Givoli D. Non-reflecting boundary conditions: a review. *Journal of Computational Physics* 1991; **94**: 1–29.

[4] Tsynkov SV. Numerical solution of problems on unbounded domains: a review. *Applied Numerical Mathematics* 1998; **27**: 465–532.

[5] Astley RJ. Infinite elements for wave problems: a review of current formulations and an assessment of accuracy. *International Journal for Numerical Methods in Engineering* 2000; **49**: 951–976.

[6] Givoli D. High-order local non-reflecting boundary conditions: a review. *Wave Motion* 2004; **39**: 319–326.

[7] Wolf JP. *Dynamic Soil-Structure Interaction*. Prentice-Hall, Englewood Cliffs, 1985.

[8] Wolf JP. *Soil-Structure-Interaction Analysis in Time Domain*. Prentice-Hall, Englewood Cliffs, 1988.

[9] Givoli D. *Numerical Methods for Problem in Infinite Domains*. Elsevier, Amsterdam, 1992.

[10] Wolf JP and Song Ch. *Finite-Element Modelling of Unbounded Media*. John Wiley & Sons, Chichester, 1996.

[11] Hall WS and Oliveto G. *Boundary Element Methods for Soil-Structure Interaction*. Kluwer Academic Publishers, 2003.

[12] Beskos DE. Boundary element methods in dynamic analysis. *Applied Mechanics Reviews, ASME* 1987; **40**: 1–23.

[13] Kausel E. Thin layer method: formulation in time domain. *International Journal for Numerical Methods in Engineering* 1994; **37**: 927–941.

[14] Song Ch and Wolf JP. The scaled boundary finite-element method – alias consistent infinitesimal finite-element cell method – for elastodynamics. *Computer Methods in Applied Mechanics and Engineering* 1997; **147**: 329–355.

[15] Wolf JP. Consistent lumped-parameter models for unbounded soil: physical representation. *Earthquake Engineering and Structural Dynamics* 1991; **20**: 11–32.

[16] Paronesso A and Wolf JP. Global lumped-parameter model with physical representation for unbounded medium. *Earthquake Engineering and Structural Dynamics* 1995; **24**: 637–654.

[17] Alpert B, Greengard L, and Hagstrom T. Nonreflecting boundary conditions for the time-dependent wave equation. *Journal of Computational Physics* 2002; **180**: 270–296.

[18] Ruge P, Trinks C, and Witte S. Time-domain analysis of unbounded media using mixed-variable. *Earthquake Engineering and Structural Dynamics* 2001; **30**: 899–925.

[19] Paronesso A and Wolf JP. Recursive evaluation of interaction forces and property matrices from unit-impulse response functions of unbounded medium based on balancing approximation. *Earthquake Engineering and Structural Dynamics* 1998; **27**: 609–618.

[20] Lysmer J and Kuhlemeyer RL. Finite dynamic model for infinite media. *Journal of Engineering Mechanics, ASCE* 1969; **95**: 859–877.

[21] Smith WD. A nonreflecting plane boundary for wave propagation problems. *Journal of Computational Physics* 1974; **15**: 492–503.

[22] Engquist B and Majda A. Radiation boundary conditions for acoustic and elastic wave calculations. *Communications on Pure and Applied Mathematics* 1979; **32**: 313–357.

[23] Liao ZP and Wong HL. A transmitting boundary for the numerical simulation of elastic wave propagation. *Soil Dynamics and Earthquake Engineering* 1984; **3**: 174–183.

[24] Bayliss A, Gunzburger M, and Turkel E. Boundary conditions for the numerical solution of elliptic equations in exterior regions. *SIAM Journal on Applied Mathematics* 1982; **42**: 430–451.

[25] Higdon RL. Absorbing boundary conditions for difference approximations to the multi-dimensional wave equation. *Mathematics of Computation* 1986; **47**: 437–459.

[26] Hagstrom T and Hariharan SI. A formulation of asymptotic and exact boundary conditions using local operators. *Applied Numerical Mathematics* 1998; **27**: 403–416.

[27] Grote MJ and Keller JB. Exact nonreflecting boundary condition for elastic waves. *SIAM Journal of Applied Mathematics* 2000; **60**: 803–819.

[28] Guddati MN and Tassoulas JL. Continued-fraction absorbing boundary conditions for the wave equation. *Journal of Computational Acoustics* 2000; **8**: 139–156.

[29] Thompson LL, Huan RN, and He DT. Accurate radiation boundary conditions for the two-dimensional wave equation on unbounded domains. *Computer Methods in Applied Mechanics and Engineering* 2001; **191**: 311–351.

[30] Krenk S. Unified formulation of radiation conditions for the wave equation. *International Journal for Numerical Methods in Engineering* 2002; **53**: 275–295.

[31] Givoli D and Neta B. High-order non-reflecting boundary scheme for time-dependent waves. *Journal of Computational Physics* 2003; **186**: 24–46.

[32] Hagstrom T and Warburton T. A new auxiliary variable formulation of high-order local radiation boundary conditions: Corner compatibility conditions and extensions to first-order systems. *Wave Motion* 2004; **39**: 327–338.

[33] Geers TL. Singly and doubly asymptotic computational boundaries. In Geers TL, editor, *Proceedings of the IUTAM Symposium on Computational Methods for Unbounded Domains* pages 135–141. Kluwer Academic Publishers 1998.

[34] Hagstrom T, Mar-Or A, and Givoli D. High-order local absorbing conditions for the wave equation: Extensions and improvements. *Journal of Computational Physics* 2008; **227**: 3322–3357.

[35] Geers TL. Doubly asymptotic approximations for transient motions of submerged structures. *Journal of the Acoustical Society of America* 1978; **63**: 1500–1508.

[36] Underwood P and Geers TL. Doubly asymptotic, boundary-element analysis of dynamic soil-structure interaction. *International Journal of Solids and Structures* 1981; **17**: 687–697.

[37] Geers TL and Zhang P. Doubly asymptotic approximations for submerged structures with internal fluid volumes. *Journal of Applied Mechanics* 1994; **61**: 893–906.

[38] Geers TL and Lewis BA. Doubly asymptotic approximations for transient elastodynamics. *International Journal of Solids and Structures* 1997; **34**: 1293–1305.

[39] Geers TL and Toothaker BJ. Third-order doubly asymptotic approximations for computational acoustics. *Journal Computational Acoustics* 2000; **8**: 101–120.

[40] Bazyar MH and Song Ch. A continued-fraction-based high-order transmitting boundary for wave propagation in unbounded domains of arbitrary geometry. *International Journal for Numerical Methods in Engineering* 2008; **74**: 209–237.

[41] Givoli D. Recent advances in the DtN FE method. *Archives of Computational Methods in Engineering* 1999; **6**: 71–116.

[42] Engquist B and Majda A. Absorbing boundary conditions for the numerical simulation of waves. *Mathematics of Computation* 1977; **31**: 629–651.

[43] Higdon RL. Numerical absorbing boundary conditions for the wave equation. *Mathematics of Computation* 1987; **49**: 65–90.

[44] Birk C and Ruge P. Representation of radiation damping in a dam-reservoir interaction analysis based on a rational stiffness approximation. *Computers and Structures* 2007; **85**: 1152–1163.

[45] Harari I and Djellouli R. Analytical study of the effect of wave number on the performance of local absorbing boundary conditions for acoustic scattering. *Applied Numerical Mathematics* 2004; **50**: 15–47.